Defect formation during a continuous phase transition

2009 EPL 87 66003

(http://iopscience.iop.org/0295-5075/87/6/66003)

A Letters Journal Exploring the Frontiers of Physics

September 2009

EPL, **87** (2009) 66003
doi: 10.1209/0295-5075/87/66003

www.epljournal.org

Defect formation during a continuous phase transition

A. D. Pezzutti[1,2], L. R. Gómez[1], M. A. Villar[2] and D. A. Vega[1(a)]

[1] *Department of Physics and Instituto de Física del Sur, IFISUR (UNS-CONICET) Além 1253, 8000 Bahía Blanca, Argentina*
[2] *Planta Piloto de Ingeniería Química, PLAPIQUI (UNS-CONICET) - Bahía Blanca, Argentina*

received 27 July 2009; accepted in final form 9 September 2009
published online 12 October 2009

PACS 64.60.Bd – General theory of phase transitions
PACS 61.72.Bb – Theories and models of crystal defects
PACS 98.80.Cq – Particle-theory and field-theory of the early Universe (including cosmic pancakes, cosmic strings, chaotic phenomena, inflationary universe, etc.)

Abstract – We study the process of defect formation during a continuous phase transition in an off-critical system. We focus on the spinodal-assisted nucleation regime, where the continuous amplification of density fluctuations induces the pseudo-nucleation of the equilibrium phase. The collision of the different propagating domains produces a domain structure with average domain size and density of defects strongly dependent on the cooling rate. The distribution of the topological defects is in good agreement with the cosmological Kibble-Zurek model proposed to determine the creation of topological defects during a symmetry-breaking phase transition.

Introduction. – Symmetry-breaking phase transitions are a quite common phenomenon encountered in a large number of fields, including condensed matter, statical and particle physics [1–3]. One of the most impressive phase transitions is, perhaps, the formation of the early Universe. It has been proposed by different theories that just after the Bing Bang the Universe underwent several phase transformations that selected the current broken-symmetry state, with its particular interactions and elementary particles. As originally pointed out by Kibble in 1976, one of the possibilities to test those theories would be to look at the primitive topological defects associated with the symmetry-breaking phase transitions in the early Universe [3]. Due to relativistic causality, cosmological phase transitions inevitably lead to the formation of topological defects [4]. In this context, important questions about the mechanism of defect formation and their dynamics have naturally emerged. In order to estimate the initial density of defects at the early Universe, Kibble estimated the correlation length ξ in a symmetry-breaking phase transition [3]. One decade after Kibbles's model, Zurek argued that during a continuous phase transition ξ should be dominated by non-equilibrium aspects of the phase transition [5]. As a consequence of the critical slowdown (the divergence of the relaxation time as the system approach to the critical temperature), a continuously cooled system would not be able to equilibrate and become out of equilibrium. In 1985 Zurek proposed to test the theory of cosmological phase transitions in condensed-matter systems [5]. Since then, the Kibble-Zurek theory has been tested in a wide variety of physical systems [4], including liquid helium [6,7], liquid crystals [8,9], superconductors, Josephson junctions [10] and convection patterns [11]. Thus, the Kibble-Zurek model is a universal theory for the dynamics of defect formation whose applications range from the transitions in the grand unified theories of high-energy physics to the phase transitions observed in different condensed-matter systems [5].

Although equilibrium properties of topological defects in different condensed-matter systems has been well established during the last century [1], still little is known about the dynamic mechanisms leading to their formation at the onset of phase transitions. It should be noted that the interest in the distribution and features of the topological defects is not only of importance from a basic point of view. An incredible variety of materials employed in everyday life are obtained through symmetry-breaking phase transitions. During these transitions the formation of defects is completely unavoidable. Since these defects have a profound effect over the mechanical, transport and optical properties, its control have an enormous technological importance.

Recently, we have shown that the Cahn-Hilliard approach can be used as a toy model to test the process of

(a) E-mail: dvega@criba.edu.ar

spinodal-assisted nucleation. Even though the process of phase separation was conducted in the spinodal region, it was found that the structure of density fluctuations acts like a precursor for the formation of ordered structures with long-range orientational and translational order, resembling the crystalline structures found in the nucleation and growth regime [12]. Then, this is an ideal model to test the current theories of defect formation.

In this work we study the process of defect formation through a Cahn-Hilliard model with competing short- and long-range interactions in a region of the phase diagram where the dynamics is controlled by the critical slowing-down. In our case, the equilibrium low-temperature phase is constituted by domains with crystalline structure. We focus in the spinodal-nucleation region, where the continuous relaxation of the order parameter produces the nucleation and propagation of the equilibrium phase.

Model. – There are many systems in nature where the free energy includes short-range attractive and long-range repulsive interactions. Examples includes Langmuir films, magnetic garnets or block copolymers. In this case, if the order parameter is conserved and in the neighborhood of the critical point the dynamical response during a phase transition can be phenomenologically described by the following Cahn-Hilliard dynamics [13,14]:

$$\frac{\partial \psi}{\partial t} = M\nabla^2 \left\{ \frac{\delta F}{\delta \psi} \right\}, \tag{1}$$

where M is a mobility coefficient and the free energy $F(\psi)$ is given by

$$F = \int \mathrm{d}\mathbf{r}^3 \left[U(\psi) + \frac{D}{2}(\nabla\psi)^2 \right] + \frac{\beta}{2} \int \mathrm{d}\mathbf{r}'^3 G(\mathbf{r}-\mathbf{r}')\,\psi(\mathbf{r})\,\psi(\mathbf{r}'). \tag{2}$$

Here $\psi(\mathbf{r})$ is the order parameter field, $G(\mathbf{r})$ is a solution of $\nabla^2 G(\mathbf{r}) = -\delta(\mathbf{r})$, and $U(\psi) = -\frac{1}{2}\tau(t)\psi^2 + \frac{1}{3}\nu\psi^3 + \frac{1}{4}\kappa\psi^4$ is the typical Guinzburg-Landau asymmetric double well. The parameters β, ν, κ and D are phenomenological constants, and $\tau(t)$ provides a measurement of the depth of quench as a function of time. In the spinodal region, the double-well shape of $U(\psi)$ favors the formation of periodic profiles with well-defined wavelength and symmetry. While in three-dimensional systems this model can led to different crystalline structures like lamellae, hexagonally packed cylinders, spheres arranged on body-centered cubic lattice or a bicontinuous structure with $Ia\bar{3}d$ space-group symmetry, in two dimensions the smectic or hexagonal phases are the preferred low-temperature low-symmetry phases. We can note that in the case of an instantaneous quench, eq. (1) leads to spinodal decomposition for temperatures $\tau > \tau_s = 2\sqrt{\beta D}$, being τ_s the spinodal temperature.

Here we study the dynamical process of defect formation during the continuous transition from an homogeneous high-temperature phase towards the equilibrium hexagonal phase ($\nu \neq 0$). The thermal treatment employed includes an instantaneous quench from the disordered phase into the spinodal line. Then, the system is continuously cooled inside the spinodal region at a given cooling rate. For simplicity we employed a linear dependence of the depth of quench with time: $\tau(t) = \tau_s + V_q t$. Through this thermal treatment we completely prevent any nucleation of the equilibrium phase via the nucleation and growth mechanism. The initial state was modelled by Gaussian random fluctuations of the order parameter and the temporal evolution was obtained by solving eq. (1) through a finite differences scheme. For comparison, we have also analyzed the process of phase separation during an isothermal treatment at depths of quench below the spinodal ($\tau > \tau_s$). Although our simulations do not include thermal noise during the temporal evolution, we have found that the main findings of this work are independent of the fluctuations[1].

Linear instability analysis. – At short times the order parameter $\psi_{early} \sim 0$ and the early-time evolution of the system can be obtained through the linear approximation of eq. (1). Then, the stability of the homogeneous high-temperature state can be studied by considering the order parameter as $\psi_{early} = \int \mathrm{d}\mathbf{k} A_{\mathbf{k}}(t) \exp(i\mathbf{k}\cdot\mathbf{r})$, where $A_{\mathbf{k}}(t)$ is the initial amplitude of the $\mathbf{k}$-mode. The time dependence of $A_{\mathbf{k}}(t)$ is found by substituting ψ_{early} into eq. (1):

$$A_{\mathbf{k}}(t) = A_{\mathbf{k}}(0) \exp\left\{ \int_0^t \mathrm{d}t' [-Dk^4 + \tau(t')k^2 - \beta] \right\}. \tag{3}$$

Then, similarly to isothermal decomposition, the continuous cooling also results in the selective amplification of a narrow band of growing modes (modes outside the ring of unstable k's are exponentially damped). The strong selectivity of modes can be clearly observed in fig. 1, where we plotted $\lambda(k,t) = \int_0^t \mathrm{d}t' [-Dk^4 + \tau(t')k^2 - \beta]$ as a function of t and k at different cooling rates. Note that at a given time, when the system overpass the critical quench ($\tau \sim \tau_s$) the range of unstable modes ($\lambda(k,t) > 0$) is smaller as the cooling rate is reduced. As will be shown in the next sections, the width of the band of unstable modes is very important because it defines the features of the system at longer times. This strong mode selectivity has a direct influence in both, the correlation length and the density of topological defects.

Pre-transitional state. – The time spanned since the system goes through the spinodal line until the non-linearities start to dominate the dynamics allows us to define an incubation time t_i where the kinetic is dictated by the linearized approximation of eq. (1). For slow cooling rates the competing interactions select a narrow range of unstable modes and the early order parameter can be expressed as a random superposition of modes with

[1] Here thermal fluctuations only renormalize the depth of quench without affecting the relaxational mechanisms and scaling laws.

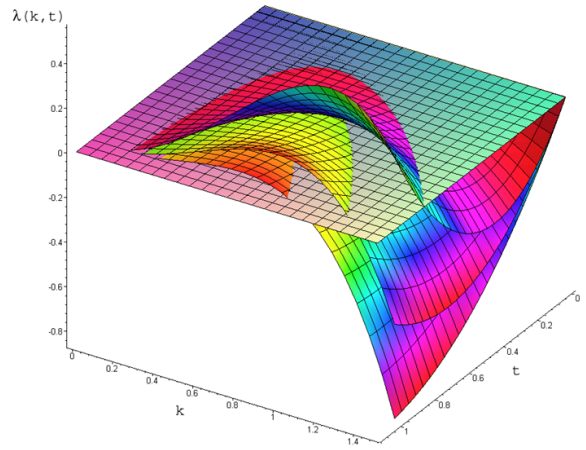

Fig. 1: (Color online) $\lambda(k,t)$ at three different cooling rates. At a given time scale, there is a strong k selectivity at slow cooling rates. The plane represents the isothermal spinodal.

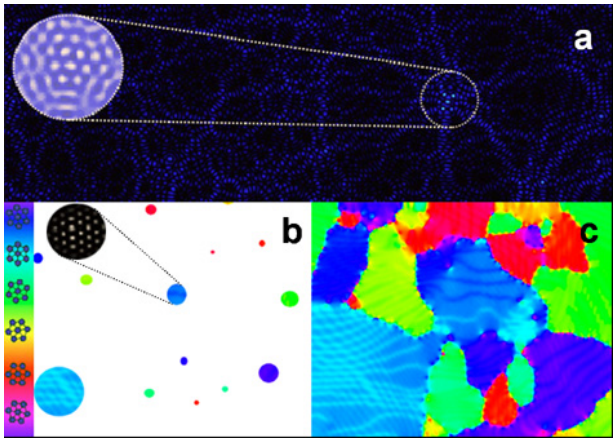

Fig. 2: (Color online) a) Filamentary network of density fluctuations. b) Pseudo-nucleation of the equilibrium phase as seen through the oreintational field (color scale on the left). c) Domain structure at long times.

a roughly fixed wave vector amplitude k_0, but random amplitudes, phases and directions. That is, since $\lambda(k,t)$ is sharp peaked at k_0 we can further approximate ψ_{early} as $\psi_{early}(\mathbf{r},t) \sim \int \mathrm{d}\Sigma A_{\mathbf{k}_0}(t) \exp(i\mathbf{k}_0 \cdot \mathbf{r})$.

Then, when the length scale selectivity is very strong thermal fluctuations with wavelength scales outside the ring of unstable modes, determined by the dominating wave vector k_0, are exponentially suppressed. During this early period of time the order parameter can be reasonably well described by ψ_{early} until the linearized approximation of eq. (1) breaks down.

In a previous paper we have shown that the length scale selectivity conducted by the spinodal process during an isothermal treatment led to the formation of a filamentary network of density fluctuations that resemble the scarred states found in other physical systems [12]. From quantum chaos and related fields it is well known that the random superposition of sinusoidal waves with constant wavelength amplitude results in a filamentary network of fluctuations [15]. These ridged structures are a general wave phenomenon and they are present in systems where the dynamics is represented as a random superposition of modes. Since in our model we can have a strong length scale selectivity, we can expect the emergence of similar patterns to those observed in isothermal treatment, *i.e.*, a network of ridges with large amplitude fluctuations.

Figure 2(a) shows a typical pre-transitional state observed during the incubation time for a system slowly cooled into the spinodal region. As previously pointed out, this pattern resembles those found during isothermal decomposition [16]. Then, similarly to isothermal treatments, here we can expect that by increasing the cooling rate the pattern of the early density fluctuations becomes strongly affected by the increase in the number of unstable modes. We have observed that during the incubation period the long-range correlations produced by the ridges disappear when the system is cooled at a high cooling rate. This effect onto the network of ridges is a mere consequence of the increase of the band of unstable modes during the incubation time [16]. Thus, for rapid cooling the early fluctuations form a disordered network without long-range correlations.

Pseudo-nucleation mechanism. – As a consequence of the continuous amplification of ψ, as time proceeds, the non-quadratic terms in $U(\psi)$ acquires a larger relative importance and the linearized approximation involved solving eq. (1) breaks down. This linearization is valid during the incubation time, just after the onset of the spinodal instability and before the mean field $\langle\psi^2\rangle$ becomes large enough to trigger the non-linear effects. Although this non-linear effects are triggered uniformly through the system, at slow cooling rates the presence of the filamentary network of ridges controls the pseudo-nucleation of the stable phase. Since in our case the mechanism of nucleation and growth is completely inhibited by the thermal treatment, the inhomogeneities in the nucleation of the equilibrium phase are dictated by the strong length scale selectivity.

The presence of the ridged structure observed if fig. 2(a) indicates that although there is a continuous amplification of the order parameter in the whole system, it amplifies faster at regions with initially larger fluctuations, *i.e.*, ridges. Then, since the non-linearities define the crystalline symmetry of the equilibrium phase, preferentially amplified ridges trigger the nucleation of well-ordered domains that rapidly propagates throughout the system. In our case, the phase of equilibrium is constituted by an array of hexagonally packed domains.

Previously it was found that the equilibrium phase is pseudo-nucleated at those points with the larger order parameter fluctuations and lower symmetry, that is, at the branching points of the network of ridges [12]. During the incubation time, the low symmetry around

the branching points induces the preferential appearance of the non-linearities in the dynamics and then, the nucleation of seeds with the right symmetry. In fig. 2(a) we have emphasized the presence of one of this precursors for the pseudo-nucleation of the equilibrium phase. While in the seeds there is a continuous amplification of the order parameter until saturation, the front of the growing crystals propagates through the system at a time-temperature–dependent velocity. Although the process of pseudo-nucleation can be analyzed through the order parameter ψ, it is more convenient to analyze it through the orientational field. Standard image processing techniques were employed to identify the center of each disk in the hexagonal pattern. Then, a Delaunay triangulation is used to determine the inter-bond orientation between near-neighbor disks $\theta(\mathbf{r})$ [16,17]. In figs. 2(b) and (c) we plotted the orientational field of the crystalline structure $\theta(\mathbf{r})$ at two different time scales (the color code employed to identify $\theta(\mathbf{r})$ is shown on the left of fig. 2(b)). In fig. 2(b) we can observe the pseudo-nucleation and propagation of orientationally uncorrelated domains, while in fig. 2(c) the collision between the different propagation domains leads to a frozen domain structure with a domain size controlled by the cooling rate. While the order parameter at those regions where the non-linearities have not been triggered is small and still dictated by the linear response, in the interior of the propagating seeds the order parameter is close to saturation (equilibrium). Then, these coherent structures can propagate freely through the system until they collide with other growing domains. Since the orientation of distant growing crystals is uncorrelated, the collision between the different domains leads to a structure of domains with a characteristic domain size ξ (fig. 2(c)).

Domain collision and Kibble-Zurek mechanism for defect formation. – At the time scale of the incubation time the linearized approximation of eq. (1) breaks down and the dynamics rapidly becomes frozen as a consequence of the continuous cooling. At this time scale the collision between domains produces Peierls-like barriers that prevent the equilibration of the system [17] and the domain structure remains completely frozen. This freezing-out of the systems dynamics can be related to the Zurek time t_z [5]. Figure 3 shows the Zurek time (or induction time) as a function of the cooling rate. While for isothermal conditions the kinetics in the neighborhood of the spinodal is dominated by the critical slowing-down, with incubation times diverging as τ_r^{-1}, here the Zurek time t_z ($t_z \sim t_i$) is controlled by V_q. The onset of the non-linear dynamics during continuous cooling can be determined through $\langle\psi^2\rangle = 1/\Omega \int_\Omega \psi(\mathbf{r})^2 \, \mathrm{d}\mathbf{r}$ as the time at which $\langle\psi^2\rangle$ reach half of its value of saturation (although other values can be used, once triggered, the process of grain propagation is so fast that the scaling of t_z with V_q is quite insensitive to this particular choice). The inset of fig. 3 shows $\langle\psi^2\rangle$ as a function of time. In this

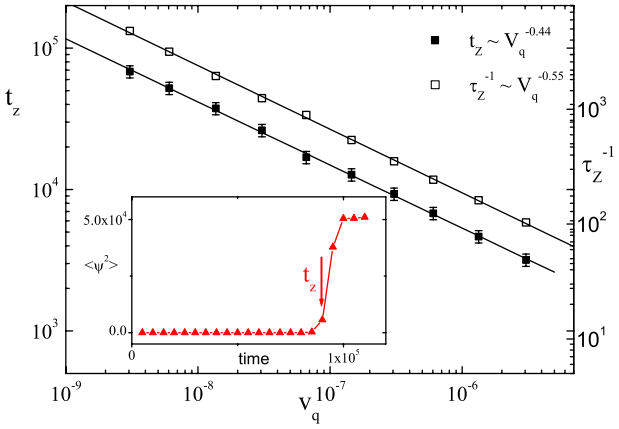

Fig. 3: (Color online) Zurek's time and temperature as a function of V_q. The inset shows through $\langle\psi^2\rangle$ the onset of non-linear dynamics.

figure it can be observed that $\langle\psi^2\rangle$ rapidly reaches its saturation value after the non-linear dynamics comes into play (at $t \sim t_z$). The onset of the non-linear dynamics can be also determined through the amplification factor $\lambda(k,t)$. In this case, non-linearities are triggered at a time dictated by $V_q t^2 \sim 1$, *i.e.*, $t \sim V_q^{-1/2}$. Figure 3 shows that t_z follows a scaling law with a scaling exponent close to 1/2 ($t_z \sim V_q^{-0.44}$), in good agreement with the scaling predicted according to the breaks down of the linearized approximation.

As a consequence of the formation of perfectly ordered domains the totality of the topological defects is located at the interfaces of the domains. This feature marks an important difference with other systems where it is quite difficult to prevent the formation of local distortions and defects in regions other than interfaces. Any mechanism in the nucleation and growth regime involves seeds with a different symmetry than that corresponding to equilibrium or the presence of anisotropies that deeply affect the degree of order of the growing domains.

In our system the topological defects are constituted by positive and negative vortexes (disclinations in the jargon of liquid crystals) [1]. For positive (negative) vortexes the orientational field θ twist to a non-trivial value of $\oint \Delta\theta = +\pi/3$ ($\oint \Delta\theta = -\pi/3$). Figures 4(a) and (b) show the vortex found in our system, as seen through $\theta(r)$. In this system most of these defects forms pairs of vortex-antivortex dipoles arranged along the domain walls (fig. 4(c)). In the state of lowest energy, these dipoles are separated by an small distance ($\sim 1/k_0$). Note that while isolated vortexes produce highly energetic long-range distortions in the orientational field (with a free energy diverging as $\ln(r)$) in our system the distortions associated to the defects are short ranged and the excess in the free energy is located at the domain walls. Then, even the orientational distortions generated by the free vortexes are short ranged. We have found isolated vortexes (vortex not engaged in a dipole) at domain walls and triple points, that is, at the point where three grains collide.

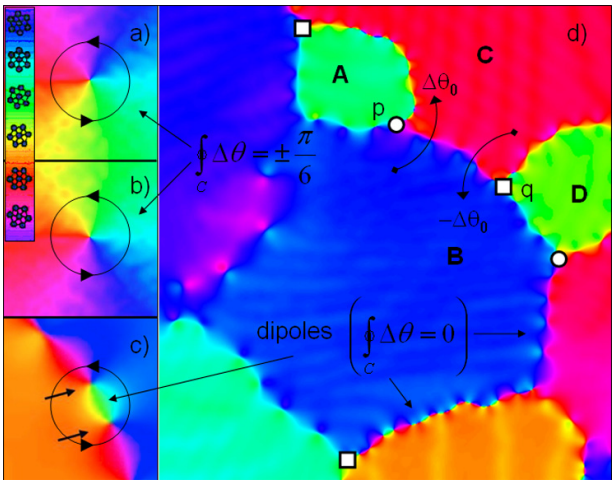

Fig. 4: (Color online) Typical topological defects found in the hexagonal system. a) Positive disclination. b) Negative disclination. c) Dipole of vortexes (dislocation). Note that the long-range orientational field of the vortexes becomes short ranged when they are arranged into a dipole. d) Domain structure and representative defects. The circles (squares) indicate positive (negative) vortexes. At the bottom of this figure we have emphasized an array of dipoles of vortexes.

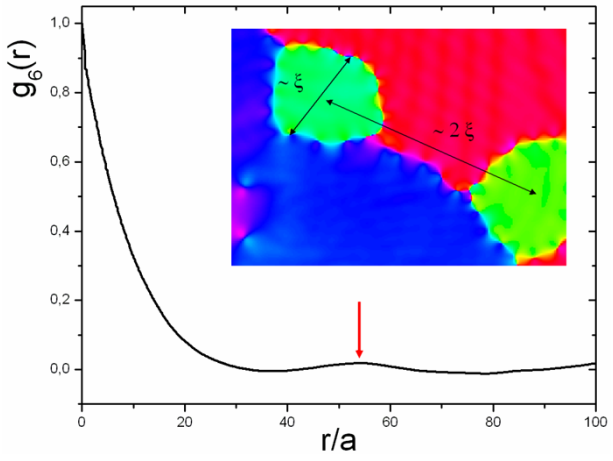

Fig. 5: (Color online) Orientational correlation function $g_6(r)$. Note the presence of an small maximum (arrow) indicating the appearance of orientational correlations between grains separated by a distance $\sim 2\xi_6$ (inset).

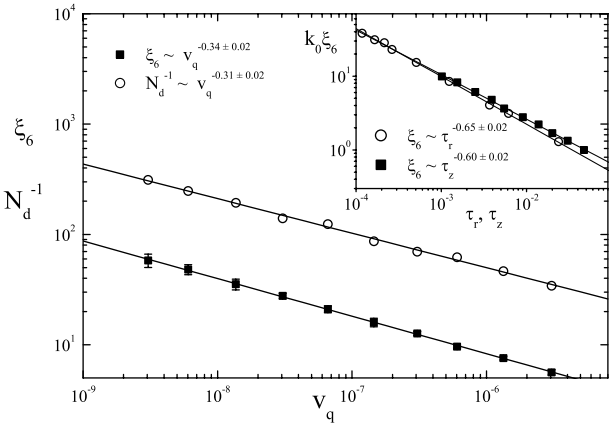

Fig. 6: Correlation length ξ_6 and N_d^{-1} as a function of the cooling rate V_q. The inset shows $k_0\xi_6$ as function of τ_r for the isothermal treatment and as a function of τ_z for the continuous cooling.

In fig. 4(d) we have indicated representative defects found at the domain walls and triple points.

Interestingly, as pointed out by Ray and Srivastava, near-neighbor triple points can induce the formation of correlated vortex-antivortex pairs separated by a distance of the order of the domain size [18]. This correlation can be observed in fig. 4 and its origin can be understood as follows. Let p be a vortex located at the intersection of three domains, like the vortex located at the intersection between domains A, B and C in fig. 4. The presence of a vortex at p originates a partial winding of θ from domain B to domain C. This partial winding of θ between B and C introduces a preferential winding to locate an antivortex at q. Then, the existence of the partial winding at triple points is the source of the vortex-antivortex correlations observed in fig. 4.

Since the domains are perfectly ordered, a good approximation of the average domain size can be obtained through the orientational correlation length ξ_6. In our case, this correlation length can be determined by fitting the azimuthal averaged orientational correlation function $g_6(r) = \langle \exp[6i(\theta(\mathbf{r}) - \theta(\mathbf{r}'))] \rangle$ through a single exponential: $g_6(r) \sim \exp(-r/\xi_6)$. Figure 5 shows the orientational correlation function for a system slowly cooled into the spinodal region. Note that although at short distances $g_6(r)$ decays exponentially, at distances beyond the average domain size there is a small maximum in the orientational correlation function. The presence of this maximum is related to the orientational correlations generated by the collision of domains and can be correlated to the vortex-antivortex correlations previously discussed.

In order to quantify the effect of the cooling rate on the mechanism of defect formation, in fig. 6 we plot the orientational correlation length ξ_6 and the density of free vortex N_d as a function of the cooling rate V_q. Here, by free vortex we mean defects not involved in a dipole.

Note that by increasing the cooling rate there is a reduction in the average domain size and consequently, an increasing density of topological defects. This figure shows that both ξ_6 and N_d follow a power law with the cooling rate V_q. While ξ_6 decreases with the cooling rate as $\xi_6 \sim V_q^{-1/3}$, the density of defects increases as $N_d \sim V_q^{1/3}$. This scaling relationships can be understood in terms of Zurek's arguments. During a continuous phase transition the correlation length diverges with the critical parameter as $\xi \sim \tau_r^{-\nu}$ (here $\tau_r = \tau/\tau_s - 1$, where τ is the depth of the quench). However, due to the critical slowing-down the time required to equilibrate the system also diverges as $\sim \tau_r^{-\mu}$. Then, beyond a characteristic time the system is not be able to equilibrate, falling out of equilibrium

and freezing. The correlation length at this time will be the average domain size and will scale with the cooling rate as $\xi \sim V_q^{-\nu/(\mu+1)}$. Here, through the induction time t_z we can determine the depth of quench at which the dynamics becomes frozen (Zurek depth of quench τ_z) as $\tau_z = V_q t_z$. Figure 3 also shows τ_z as a function of V_q. We found that τ_z follows a power law with V_q with an exponent close to 1/2. According to the data of fig. 3 and fig. 6, we have power laws consistent with $t_z \sim V_q^{-1/2}$ and $\xi_6 \sim V_q^{-1/3}$. This implies that in our system we have $\nu \sim 2/3$ and $\mu \sim 1$, which is consistent with the predictions of the renormalization group approach and experiments [19] (in ref. [12] we have shown that during an isothermal treatment the induction time for pseudo-nucleation diverges with an exponent $\mu = 1$).

In the inset of fig. 6 we compare the correlation length obtained during isothermal treatment and continuous cooling as a function the effective depth of quench. In the case of isothermal treatment the depth of quench is directly τ_r, while for continuous cooling we have employed τ_z. During isothermal treatments we have found that the correlation length follows the scaling with the reduced temperature τ_r consistent with $\xi_6 \sim \tau_r^{-2/3}$. In this case, the critical slowing-down imposes that the incubation time diverges as $\sim \tau_r^{-1}$. On the other hand, when the orientational correlation length is plotted against τ_z, it was found that it also follows a power law with a slightly smaller exponent $\xi_6 \sim \tau_z^{-0.6\pm0.02}$. In addition, it is also noted that similar correlation lengths are obtained through both thermal treatments when they are evaluated at temperatures that control the critical slowing-down (τ_r or τ_z for isothermal or continuous cooling, respectively). The small but systematic difference between both thermal treatments are a clear signature of the length scale selectivity. As compared with isothermal treatments, during a continuous cooling the initial stage of phase separation produces a stronger length scale selectivity that increases the average domain size and consequently, reduces the density of topological defects.

When the process of vortex formation is completely random, we can expect that the correlation length and the density of vortex become linked trough $\xi_6 \sim N_d^{-2}$. However in our system the majority of the free defects are vortexes located at the domain walls and the density of defects and correlation length must be related as $\xi_6 \sim N_d^{-1}$. Here this implies that $N_d \sim V_q^{1/3}$. In fig. 6 we have also plotted the number of free vortexes as a function of the cooling rate. Note that $N_d \sim V_q^{0.31\pm0.02}$, which is consistent with a vortex density dominated by domain walls rather than by triple points and in good agreement with the experimental data of Casado *et al.* in a Bénard-Marangoni convection system [11].

Conclusions. – In summary, we have observed that the strong length selectivity may lead to the appearance of an early network of density fluctuations that acts as a precursor for nucleation. In qualitative agreement with the Kible-Zurek picture for cosmological phase transitions, once triggered, the domains propagate free of any orientational or translational distortions. Then, the totality of the orientational defects are condensed along domain boundaries and their density is entirely controlled by the cooling rate. Although the dominating defects are dipoles in the ground state, there are also free vortexes located at domain walls and triple points. However, the scaling of the number of defects with the correlation length indicates that the largest population of free vortexes are located at domain walls.

* * *

This work was supported by the National Research Council of Argentina (CONICET), Universidad Nacional del Sur and the ANPCyT (PICT 22-38462).

REFERENCES

[1] Chaikin P. M. and Lubensky T. C., *Principles of Condensed Matter Physics* (Cambridge University Press) 1995.
[2] Gunton J. D., San Miguel M. and Sahni P. S., in *Phase Transitions and Critical Phenomena*, edited by Domb C. and Lebowitz J. L., Vol. **8** (Academic Press, London) 1983, p. 267.
[3] Kibble T. W. B., *J. Phys. A: Math. Gen.*, **9** (1976) 1387.
[4] Kibble T. W. B., *Phys. Today*, **60**, issue No. 9 (2007) 47.
[5] Zurek W. H., *Nature*, **317** (1985) 505.
[6] Bauerle C., Yu M., Bunkov S. N., Fisher H., Godfrin G. R. and Pickett, *Nature*, **382** (1996) 332.
[7] Ruutu V. M. H., Eltsov V. B., Gill A. J., Kibble T. W. B., Krusius M., Makhlin Y. G., Placais B. and Volovik G. E., *Nature*, **382** (1996) 334.
[8] Chuang I., Durrer R., Turok N. and Yurke B., *Science*, **251** (1991) 1336.
[9] Bowick M. J., Chandar L., Schiff E. A. and Srivastava A. M., *Science*, **263** (1994) 943.
[10] Monaco R., Aaroe M., Mygind J., Riviers R. J. and Koshelets V. P., *Phys. Rev. B*, **74** (2006) 144513.
[11] Casado S., González-Viñas W., Mancini H. and Boccaletti S., *Phys. Rev. E*, **63** (2001) 057301.
[12] Vega D. A. and Gómez L. R., *Phys. Rev. E*, **79** (2009) 051607.
[13] Ohta T. and Kawasaki K., *Macromolecules*, **19** (1986) 2621.
[14] Seul M. and Andelman D., *Science*, **267** (1995) 476.
[15] O'Connor P., Gehlen J. and Heller E. J., *Phys. Rev. Lett.*, **58** (1987) 1296.
[16] Vega D. A., Harrison C. K., Angelescu D. E., Trawick M. L., Huse D. A., Chaikin P. M. and Register R. A., *Phys. Rev. E*, **71** (2005) 061803.
[17] Gómez L. R., Vallés E. M. and Vega D. A., *Phys. Rev. Lett.*, **97** (2006) 188302.
[18] Ray R. and Srivastava A. M., *Phys. Rev. D*, **69** (2004) 103525.
[19] Zurek W. H., *Phys. Rep.*, **276** (1996) 177.